



Electron transfer studies on Cu(II) complexes bearing phenoxy-pincer ligands

Axel Klein^{a,*}, Katharina Butsch^a, Jörg Neudörfel^b

^a Universität zu Köln, Department für Chemie, Institut für Anorganische Chemie, Greinstrasse 6, D-50939 Köln, Germany

^b Universität zu Köln, Department für Chemie, Institut für Organische Chemie, Greinstrasse 4-6, D-50939 Köln, Germany

ARTICLE INFO

Article history:

Received 3 February 2010

Received in revised form 31 May 2010

Accepted 8 June 2010

Available online 15 June 2010

Keywords:

Oxido-pincer ligands (O,N,O ligands)

Coordination chemistry

Electrochemistry

Acid–base-properties

EPR spectroscopy

ABSTRACT

Oxido-pincer ligands with phenolate-groups [2,6-bis(2-methoxyphenyl)pyridine (LOMe₂), 2,6-bis(2-hydroxyphenyl)-pyridine (LOH₂), 2,6-bis-(2,4-dimethoxyphenyl)-pyridine (LOMe₄)] coordinate to Cu^{II} forming binuclear complexes which can be easily and reliably converted into mononuclear species. Their physical properties were analysed using EPR, optical spectroscopy and (spectro-)electrochemical methods. The results were compared to those of related Ni^{II} complexes and discussed in view of Cu-containing metalloenzymes. Due to the ligands flexibility the Cu^{II}/Cu^I redox couple exhibits high reversibility, while the ligand-centred oxidation leads to highly reactive phenoxy radicals. Reduction of the LOH₂ complex leads to sequential deprotonation. The ligand LOMe₄ and the derived complexes show blue luminescence, which can be rationalised from its molecular structure (analysed by XRD).

© 2010 Elsevier B.V. All rights reserved.

1. Introduction

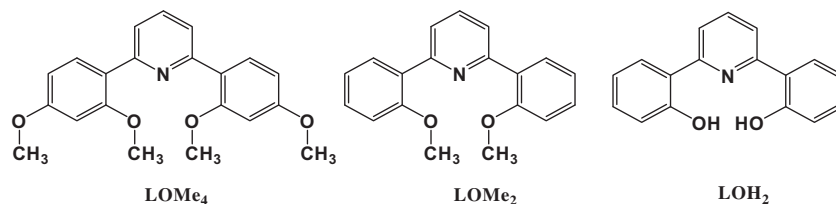
Copper is an important metal for oxidation catalysis in biological systems. Blue copper proteins (e.g., azurin or plastocyanin), tyrosinase, amine oxidase, L-ascorbate oxidase, cytochrome C oxidase, galactose oxidase (GO) and catecholase are just a few examples for copper containing enzymes. The copper ions in these enzymes are able to catalyse electron transfer of one electron (e.g., blue copper proteins [1]), two electrons (e.g., GO [2] or catecholase [3]) or four electrons (e.g., ascorbate oxidase [4]). Ascorbate oxidase and catecholase both transfer more than one electron due to the number of copper atoms per active centre (two or four, respectively), while GO contains one copper atom linked to a secondary “built-in” co-factor, a tyrosyl-radical ([Tyr]^{•+}) which accepts the second electron. Therefore, GO is able to catalyse the oxidation of terminal alcohols to the corresponding aldehydes along with the formation of hydrogen peroxide [5]. The copper atoms in these metalloenzymes change their redox state (Cu^I/Cu^{II}) reversibly and rapidly, which is important for efficient electron transfer [6]. The Cu^{II}/Cu^I mediated electron transfer reactions occur at low potentials, e.g., the copper redox couple of GO has a potential of 0.16 V versus NHE and the oxidation potential of the tyrosyl-radical is 0.41 V versus NHE [7]. This corresponds to −0.24 V (Cu^{II}/Cu^I reduction) and 0.01 V (ligand oxidation [L^{•+}]) versus FeCp₂/FeCp₂⁺ [8]. The low redox potentials in natural enzymes are always linked with unusual coordination geometries and strongly distorted coordination polyhedra, the so called entatic

state [9]. Complex systems designed to model enzyme functions have to spotlight on the coordination geometry and the resulting electrochemical properties. Suitable models need a flexible copper coordination and ligands that exhibit ligand to metal interactions [10] supporting the ³O₂ affinity of Cu^I [11] which is necessary for biological catalytic oxidation reactions.

Recently we reported on a number of complexes containing O,N,O-pincer ligands derived from 2,6-bis(hydroxymethyl)pyridine [12]. These oxido-pincer ligands bind (in their protonated forms) in a tridentate mode, forming two five-membered coplanar rings in complexes [(O,N,O)CuCl₂] or [(O,N,O)₂Cu]²⁺ [12]. This motivated us to extend our studies to phenoxido-pincer-ligands as depicted in Scheme 1. These ligands can bind through two six-membered chelates, which should allow effective binding combined with strong ligand distortion. As recently shown for Cu^{II} the size of the O,N,O binding site in 2,6-bis-(2'-hydroxyphenyl)pyridine is far too small to allow a coplanar ligand arrangement of the three aryl rings [13]. As a result the coordination flexibility in such ligands should be higher and a fast conformation change associated with the change of the redox state (Cu^{II} to Cu^I) should be possible. Therefore, complexes of such phenolate-pincers ligands are promising candidates for the modelling of bio-inspired oxidation catalysts. In this paper we report on the syntheses of phenoxido-pincer ligands (Scheme 1) and their complexes with Cu^{II} and Ni^{II}. LOH₂ is the only ligand in this series, which can alternatively bind in its protonated or deprotonated forms. Furthermore it is reasonable to assume that the deprotonation is facilitated upon coordination. Generally, acid–base properties of the redox active centre are important, since oxidation/oxygenation reactions are often associated with proton transfer. To this end, the comparison between the LOH₂ containing model system

* Corresponding author.

E-mail address: axel.klein@uni-koeln.de (A. Klein).



Scheme 1. O,N,O oxido-pincer ligands used in this study. 2,6-Bis-(2,4-dimethoxyphenyl)-pyridine (LOMe₄), 2,6-bis(2-methoxyphenyl)pyridine (LOMe₂) and 2,6-bis(2-hydroxyphenyl)pyridine (LOH₂).

with its LOMe₂ derivative is worthwhile studying. The LOMe₄ ligand was introduced to this series for the electron-releasing influence of the additional methoxy substituents and its higher steric bulk. The new compounds were fully characterised spectroscopically (NMR, UV–Vis–NIR absorption, UV–Vis emission, EPR) and electrochemically. The suitability of the Cu^{II} complexes to serve as oxidation catalysts was investigated in detail by absorption spectroscopy of parent, reduced and oxidised states using spectroelectrochemical techniques and by catalytic test reactions [14].

2. Results and discussion

2.1. Syntheses and characterisation of the ligands

While the ligands 2,6-bis(2-methoxyphenyl)pyridine (LOMe₂) and 2,6-bis(2-hydroxyphenyl)pyridine (LOH₂) have been described before [13,15,16], the 2,6-bis-(2,4-dimethoxyphenyl)pyridine (LOMe₄) ligand is a new compound and was synthesised via a Kumada-coupling reaction (for details see Section 4). The LOMe₄ ligand was first isolated as a MgBr₂ complex as inferred from NMR spectroscopy and elemental analysis. The free LOMe₄ ligand was obtained by removing the MgBr₂ from the compound using a cryptand, while other methods like acidifying the system, filtration over silica or treatment with crown ether were unsuccessful. The three ligands were obtained in sufficient yields and fully characterised by elemental analysis, ¹H and ¹³C NMR spectroscopy (see Section 4), by absorption spectroscopy and cyclic voltammetry (CV). From LOMe₂ and LOMe₄ single crystals suitable for XRD were obtained from acetone solutions. The structure of LOMe₂ was solved in monoclinic Cc, while LOMe₄ crystallises in the chiral orthorhombic space group P2₁2₁2₁. This is in line with the chirality of the ligand scaffold in the solid state [17]. Fig. 1 shows the two molecular structures (for details of the LOMe₄ crystal measurement see Supporting information).

The crystal structure of LOMe₂ has been reported in the monoclinic space group *Ia* together with the crystal structure of LOH₂ [16]. Although *Ia* is a non-standard but completely equivalent setting of Cc, the parameters reported there are not identical to ours. Assuming that π -overlap between the different ring-planes is crucial for the spectroscopic and electrochemical properties of the free

ligands and their metal complexes we will focus the description of the molecular structures to the torsion angles between the ring-planes (Table 1).

In the ligand LOMe₂ both phenol rings are markedly tilted from the central pyridine ring in a way that the two methoxy groups point into different directions one lying above the pyridine ring plane and the other one below. Thus the π -overlap between the different ring-planes in LOMe₂ is negligible. In LOMe₄ both tilt angles are slightly smaller and the methoxy groups point in the same direction opposite of the binding pocket, representing a situation far from the terdentate coordination mode in metal complexes. One of the methyl groups in *p*-position is disordered (1:3). The tilt angles of the LOH₂ ligand are the smallest found in this series and the two hydroxy groups point into the same direction. In summary all three ligands exhibit molecular structures which result from steric interactions and do not represent the terdentate coordination mode. In order to coordinate in a bis-chelate manner they have to undergo conformational changes by rotating the phenyl substituents. The corresponding rotating energies are probably rather small, while on the other hand the systems might gain energy from more efficient π -delocalisation in the all-planar conformation. However, from a study on the related ligand 2-(2-hydroxy-5-methylphenyl)-6-(2-hydroxyphenyl)-pyridine (4-methyl derivative of LOH₂) and its dipyrindine Cu^{II} complex [18] it is evident that one of the phenol substituents is in a coplanar arrangement to the central pyridine core (supported by a O–H \cdots N hydrogen bond), while in the corresponding Cu^{II} complex all three rings are tilted toward each other, due to the small cavity provided by the O,N,O donor atoms (the mentioned proton fits to the cavity). Thus an all-planar configuration cannot be expected for the Cu^{II} or Ni^{II} complexes.

Table 1
Selected data of the molecular structures of LOMe₂ and LOMe₄.

Dihedral angles	LOH ₂	LOMe ₂	LOMe ₄
PlaneO1–planeN	~26 ^a	44.40(6)	35.39(9)
PlaneO2–planeN	~30 ^a	51.75(8)	40.31(9)
PlaneO1–planeO2	~51 ^a	78.92(8)	38.06(9)

^a Averaged values from three independent molecules from Ref. [16].

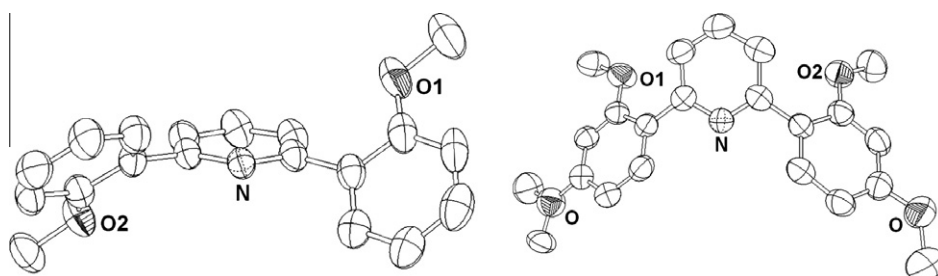
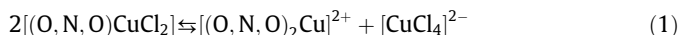


Fig. 1. View of the molecular structure of LOMe₂ (left) and LOMe₄ (right) (thermal ellipsoids represent 50% probability); the H atoms were omitted for clarity. Note that one of the methoxy groups of LOMe₄ is disordered with a 30/70 occupancy ratio.

2.2. Synthesis of the metal complexes

Our synthesis strategy for the copper complexes was mainly determined by the initial goal to generate mononuclear compounds. For deprotonated LOH_2 and related ligand types the formation of oligonuclear copper complexes with copper atoms bridged by the negatively charged oxido ligand functions (phenolates) was reported [15,16]. The oligonuclear products can be transformed to mononuclear complexes by adding suitable ligands like pyridine [18], however, this method is insufficiently controllable, due to the unknown nuclearity of the starting materials (stoichiometry) and the formation of by-products as $[\text{Cu}(\text{py})_2\text{Cl}_2]$. Therefore, we sought for more reliable strategies leading directly to mononuclear complexes. Using ligands with protonated or methoxylated oxido functions LOH_2 , LOMe_2 , LOMe_4 (Scheme 1) formation of oligonuclear species through oxido-ligand bridging is prohibited. The reaction of the three oxido-pincer ligands with CuCl_2 in methanol yielded the brown compounds $[(\text{LOMe}_2)\text{CuCl}_2]_2$, $[(\text{LOH}_2)\text{CuCl}_2]_2$ and $[(\text{LOMe}_4)\text{CuCl}_2]_2$ which were binuclear as can be inferred from their colour and EPR spectra (see below). In many reports binuclear complexes or compounds with even higher nuclearity are described to exhibit brownish colours, while monomeric derivatives are green [18]. We assume that in our dimeric products the copper atoms were octahedrally configured with two chlorido bridging ligands (Scheme 2). These solids can be dissolved in DMF resulting reliably in octahedrally configured mononuclear species $[(\text{O},\text{N},\text{O})\text{CuCl}_2(\text{DMF})]$ (Scheme 2) as indicated by their absorption spectra and EPR spectroscopy (see below).

Also in acetonitrile (MeCN) mononuclear species were obtained, however at the same time these species rapidly disproportionate following Eq. (1) in line with recent reports on related chlorido-bridged copper complexes [19] and with the previously reported pentacoordinated complexes $[(\text{RR}'\text{pydimH}_2)\text{CuCl}_2]$ ($\text{RR}'\text{pydimH}_2 = \text{oxido pincer ligands based on 2,6-bis(hydroxymethyl)pyridine}$) [12]



An alternative synthetic strategy was to perform ligand exchange reactions in acetonitrile starting from $[\text{Cu}(\text{MeCN})_4](\text{TFA})_2$ ($\text{TFA} = \text{trifluoroacetic acid}$) as a precursor. In the case of LOMe_2 no reaction took place (see Section 4), while for LOMe_4 the complex $[(\text{LOMe}_4)\text{Cu}(\text{TFA})_2]$ was obtained as a light green solid.

The LOH_2 ligand in the complex $[(\text{LOH}_2)\text{CuCl}_2]_2$, obtained from CuCl_2 and the ligand in methanol is completely protonated. It can be easily deprotonated by adding an excess of $t\text{BuOK}$ or NEt_3 to a solution of the complex in methanol. The deprotonated species $[(\text{LOH})\text{CuCl}_2]$ precipitates immediately and can be easily isolated by filtration.

In addition to Cu^{II} complexes, which were the main focus of this study, some Ni^{II} derivatives were synthesised for the sake of comparison concerning the coordination geometry (detectable by UV-Vis-NIR-, NMR- or EPR-spectroscopy) and the electrochemistry

(higher potentials for the metal-centred redox chemistry). The nickel compounds were synthesised using ligand exchange reactions starting from $[(\text{PPh}_3)_2\text{NiBr}_2]$. The obtained dimeric compounds $[(\text{LOMe}_2)\text{NiBr}_2]_2$, $[(\text{LOH}_2)\text{NiBr}_2]_2$ and $[(\text{LOMe}_4)\text{NiBr}_2]_2$ were rapidly formed but the isolated yields were low, because OPPh_3 is formed as a side product and has to be removed by recrystallisation from CH_2Cl_2 .

2.3. NMR spectroscopy

For the Cu^{II} complexes no NMR spectra could be obtained due to their paramagnetism. Ni^{II} compounds are not necessarily diamagnetic but if their geometry is square planar or distorted octahedral they are suitable for NMR-analyses. Indeed, for the dimeric complexes $[(\text{O},\text{N},\text{O})\text{NiBr}_2]_2$, ^1H NMR spectra were obtained and can be compared to spectra of the free ligands. ^{13}C NMR spectra were recorded for the free ligands (see Section 4) while low solubility of the nickel complexes did not allow such measurements.

From Table 2 it is evident that the proton signals of the ligands show remarkable low field shifts upon coordination. Especially the shifts of the pyridine ring protons indicate the metal ion coordination, while the phenol-protons are not extremely low field shifted. The observed shifts for the methoxy and hydroxy proton signals indicate that both oxido-donors are bound to the metal in any case. The spectra were found to be unchanged after days, proving the stability of the formed complexes in acetone solution.

The LOH_2 nickel complex still shows proton signals for two OH-protons, revealing that the complex formation is not connected to deprotonation of the coordinated OH-groups. However, the δ value has shifted from 9.88 to 11.67 ppm indicating that the protons are far more acidic.

2.4. EPR spectroscopy

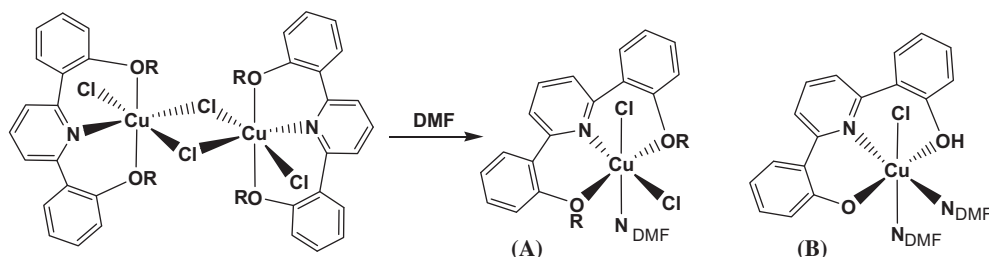
EPR spectra of all copper compounds were measured on solid samples at ambient temperatures and 110 K as well as on glassy frozen DMF solutions at 110 K (data listed in Table 3). The free ligands and nickel complexes were found to be diamagnetic. All ob-

Table 2

Selected ^1H NMR data for the free oxido-pincer ligands and their Mg^{II} and Ni^{II} complexes.^a

Compound	Py4	Py3,5	Phen6	Phen4	Phen5	Phen3	OMe/OH
LOMe_2	7.84	7.84	7.97	7.39	7.15	7.07	3.92
$[(\text{LOMe}_2)\text{NiBr}_2]_2$	8.52	8.30	8.04	7.59	7.35	7.22	4.10
LOH_2	8.00	7.72	7.69	7.35	7.05	7.00	9.88
$[(\text{LOH}_2)\text{NiBr}_2]_2$	8.00	8.00	7.86	7.32	7.00	7.00	11.67
LOMe_4	7.69	7.78	8.01		6.68	6.68	3.91/3.87
$[(\text{LOMe}_4)\text{MgBr}_2]$	8.63	8.29	6.87		6.93	8.01	4.19/3.98
$[(\text{LOMe}_4)\text{NiBr}_2]_2$	8.94	8.55	7.00		7.04	8.18	4.40/4.05

^a Chemical shifts δ in ppm, as measured in $[\text{D}_6]$ -acetone.



Scheme 2. Schematic representation of the proposed structures for the binuclear complexes $[(\text{O},\text{N},\text{O})\text{Cu}(\mu\text{-Cl})_2\text{Cu}(\text{O},\text{N},\text{O})]$ and the monomers obtained in DMF solution (A). The monomer obtained for the complex containing the deprotonated ligand LOH^- is shown in (B).

Table 3
X-band EPR data of the oxido-pincer copper complexes.^a

Compound	g_{av}	g_{\parallel}	g_{\perp}	$A_{\parallel}Cu$	Δg	Symmetry ^b	Solvent/ <i>T</i>
[(LOH ₂)CuCl ₂] ₂	2.178	2.327	2.104		0.223	OD	Solid/298 K
[(LOMe ₂)CuCl ₂] ₂	2.170	2.230	2.140		0.090	OD	Solid/298 K
[(LOMe ₄)CuCl ₂] ₂	2.158	2.333	2.070		0.263	OD	Solid/298 K
[(LOH)CuCl] ₂	2.181	2.346	2.099		0.351	OD	Solid/110 K
[(LOH ₂)CuCl ₂ (DMF)]	2.164	2.331	2.081	139 G	0.250	OE or SP	DMF/110 K
[(LOMe ₂)CuCl ₂ (DMF)]	2.166	2.336	2.081	129 G	0.255	OE or SP	DMF/110 K
[(LOMe ₄)CuCl ₂ (DMF)]	2.163	2.296	2.097	123 G	0.199	OE or SP	DMF/110 K
[(LOH)CuCl(DMF) ₂]	2.156	2.313	2.078	170 G	0.235	OE or SP	DMF/110 K
[(LOMe ₄)Cu(TFA) ₂]	2.146	2.326	2.056	165 G	0.270	OE or SP	Solid/110 K

^a g_{av} = Averaged g value = $(g_{\parallel} + 2g_{\perp})/3$; $\Delta g = g_{\parallel} - g_{\perp}$.

^b Symmetry assignment based on EPR spectroscopy (see text), OD = octahedral dimeric, OE = octahedral elongated, SP = square pyramidal.

served g values lie in the range expected for Cu^{II} complexes, while a close look reveals decent differences in the signal symmetry and subtle variations in g values and g anisotropy (Δg). The signal form of Cu^{II} is a direct hint to the complex geometry [20]. The binuclear products [(O,N,O)CuCl₂]₂ from the preparation in methanol exhibit ill-resolved axial spectra (no hyperfine splitting) and no indication of a half-field signal. Such spectra are typical for octahedrally configured chloride-bridged binuclear species (OD) [19,21]. Similar spectra have been observed also for chlorido-bridged binuclear complexes with square pyramidal surrounding of the copper ion [22,23], indicating a marginal influence of the sixth ligand [24]. A markedly different g anisotropy (Δg) is observed for the LOMe₂ complex in comparison to the other two complexes (Fig. 2), while the signal symmetry is the same. In a number of related compounds the g anisotropy reflects subtle distortions of the geometry around the copper ion imposed by the crystal structure [19,21]. Since we could not obtain crystal structures of our complexes we can only speculate, that the same mechanisms operate here. The species observed in glassy frozen DMF solutions all exhibit axial spectra with coupling constants (A_{Cu}) about 140 G for the g_{\parallel} component, which are typical for square-based pyramidal (SP), tetragonally elongated octahedral (OE) or trigonal bipyramidally (TBP) configured Cu^{II} complex [20,25–28]. The three cases can be winnowed by their g value range. TBP compounds usually have g_{\parallel} values around 2.0 and g_{\perp} around 2.2, while for the other two configurations a smallest g value >2.04 can be expected [20].

Following this classification the complexes [(O,N,O)-CuCl₂(DMF)] are mononuclear octahedrally configured complexes (Scheme 2), although we cannot rule out, that the contribution of the DMF ligand is marginal and the coordination is more of a square pyramid. The g anisotropy (Δg) is quite similar for all three complexes. The complex containing the deprotonated LOH⁻ ligand [(LOH)CuCl]₂ exhibits very similar spectra, thus we conclude that in the solid also a dimer is present. This would imply that the deprotonated oxido function takes part in the bridging between the two copper atoms. In DMF solution clear indication for a monomer complex is provided by the obtained EPR spectra. However, we

do not know if this species contains one or two DMF ligands, since assuming a square planar arrangement of the O,N,O and the Cl coligand, the presence of one or two DMF coligands in the axial position will not have marked influence on the spectroscopy. For the complex [(LOMe₄)Cu(TFA)₂] in the solid we found an axial spectrum (Fig. 2), very similar to those of the monomeric complexes with chlorido ligands and we assume a similar monomeric structure for this complex.

2.5. Luminescence properties

To further substantiate the question of tight binding, rigidity or flexibility of the ligands, we examined the emission properties of the new compounds. The ligand LOMe₄ and its complexes show blue luminescence upon irradiation into the long-wavelength absorption band (assigned to evolve from a ³ π - π excited state) in the solid and in DMF solution. Comparable emission has been reported for the Zn^{II} complex [(LO)₄(Py)₄Zn₄] in the solid state [14]. Neither in the solid, nor in DMF solution LOH₂ or LOMe₂ ligands and their complexes exhibit emission at ambient temperature. We assume that the corresponding emission for the ligands LOH₂ and LOMe₂ and their complexes is quenched by radiationless decay, and we assume that the higher distortion (from steric strain) in the free ligand LOMe₄ and its complexes compared to LOMe₂ and LOH₂ accounts for the different behaviour. The emission maxima (around 470 nm) and the Stokes shifts (around 5400 cm⁻¹) are quite similar for free LOMe₄ and its complexes, while the intensities of the emission and the quantum yields vary markedly (Table 4; representative spectra are supplied in the Supporting information). The quantum yield is higher for the magnesium compound than for the nickel and copper derivative, reflecting the better fit of the ion into the narrow binding pocket of the ligand (see discussion on the molecular structures) thus providing a rigid system (better ϕ than the free ligand). For a more detailed picture of the luminescence properties further experiments have to be carried out in the future (low-temperature measurements and time-resolved), focussing on the failure of LOH₂ and LOMe₂ and their complexes to exhibit luminescence under the applied conditions.

2.6. Electrochemical measurements

The electrochemical measurements of the copper dichlorido complexes were carried out in DMF as solvent (and *n*Bu₄NPF₆ as electrolyte) in which they were in their mononuclear form [(O,N,O)CuCl₂(DMF)]. The compound [(LOMe₄)Cu(MeCN)](TFA)₂ was measured in acetonitrile due to a better solubility. The nickel complexes, which were measured for the sake of comparison to the Cu^{II} derivatives had to be measured in THF solution since they are not completely stable in acetonitrile or DMF. The assignment of redox waves is based on the assumption that Ni^{II} and Cu^{II} complexes

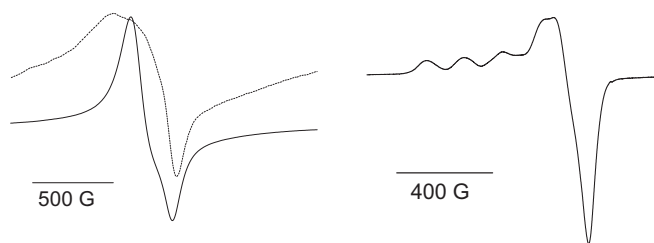


Fig. 2. X-band EPR spectra solid samples of (a) [(LOMe₂)CuCl₂]₂ (solid line) and [(LOH₂)CuCl₂]₂ (dashed line) at 298 K (left) and (b) [(LOMe₄)Cu(TFA)₂] at 298 K (right).

Table 4
Absorption, excitation and emission data of LOMe₄ and the derived metal complexes.

Compound	λ absorption maximum ^a	λ excitation maximum ^{a,b}	λ emission maximum $\lambda_{\text{exc}} = 390 \text{ nm}$	Stokes shift (cm ⁻¹)	ϕ^c
LOMe ₄	270 (21260); 298(sh) (16150); 307(sh) (17110); 313 (18160); 367 (1110)	361; 392	466	5137	0.21×10^{-3}
[(LOMe ₄)MgBr ₂]	316 (1530); 371 (550)	344(sh); 402	464	5449	3.52×10^{-3}
[(LOMe ₄)NiBr ₂ (DMF)]	318 (6600); 372 (3860)	307(sh); 380(sh); 395	467	5469	0.12×10^{-3}
[(LOMe ₄)CuCl ₂ (DMF)]	316 (14820); 371(sh) (2290); 439(sh) (330)	346; 408	475	5901	0.53×10^{-3}

^a Absorption, excitation and emission maxima in nm, intensities (in parentheses) in L mol⁻¹ cm⁻¹ as measured in DMF solution.

^b Excitation spectra obtained for the maximum emission wavelength.

^c Quantum yield.

might exhibit similar ligand-centred oxidation or reductions, while the metal-based electrochemistry should differ largely since Cu^{II} might be easily reduced (Cu^{II}/Cu^I couple), whereas for Ni^{II} oxidation (Ni^{II}/Ni^{III}) should be observable at comparably low potentials.

Indeed, the complexes under investigation show reversible reduction waves at around 0 V for the Cu^{II} complexes, while corresponding Ni^{II} complexes are oxidised at around +0.4 V (irreversibly). The irreversible ligand-centred oxidation occurs for both systems (and the free ligands) at quite similar values (0.7–1 V) (Table 5) except for the chlorido copper complex [(LOH)₂CuCl(DMF)₂] containing the deprotonated LOH⁻ ligand, for which the oxidation occurs at far lower potential. Furthermore, irreversible reduction waves were observed on cathodic scans, which were assigned to ligand-centred processes. For the complex [(LOH)₂CuCl₂(DMF)] we found waves on the reversed scan after reduction, which might be assigned to the deprotonated complex [(LOH)CuCl(DMF)₂] as referred from their potential. However, this would mean that the complex is deprotonated upon reduction. This is rather unusual, since normally one would expect a deprotonation after augmentation of positive charge (=oxidation). Essential redox potentials of the different ligands and metal complexes are summarised in Table 5 (representative CVs are supplied in the Supplementary information).

The essential electrochemical parameters for the question, if the present complexes might serve as model compounds for entatic copper enzymes are the reversibility and the potential of the Cu^{II}/Cu^I reduction wave. These potentials are markedly lower for the Cu^{II} chlorido complexes than for [(LOMe₄)Cu(MeCN)]²⁺. At the same time, the Cu^{II}/Cu^I potentials are high compared to wild-

type copper enzymes (e.g., -0.24 V for Cu^{II}/Cu^I in galactose oxidase). Furthermore, the ligand-centred oxidation occurs presumably in the coordinated phenol or phenolate, which corresponds, to enzymes containing radical co-factors and therefore transferring more than one electron (e.g., galactose oxidase). Unfortunately, the ligand oxidation processes occur irreversibly (even at high scan rates) and occur at rather high potentials, far higher than natural co-factors (e.g., 0.01 V for [Tyr]⁺ in galactose oxidase). Noteworthy, the complex containing the deprotonated ligand LOH⁻ shows a relatively low potential of 0.28 V. The reason for the very high ligand centred oxidation potentials in our complexes is very probably that the ligand systems presented herein do not have any radical-stabilising groups. Upon stabilising the radical species [L⁺] (usually by *tert*-butyl groups in 2 and 4 position of the phenolate) the compounds would not only show a reversible oxidation process, but would have also lower oxidation potentials [29].

2.6.1. Optical spectroscopy and spectroelectrochemical measurement

The complexes [(O,N,O)CuCl₂(DMF)] show typical weak ligand field (d-d) transitions around 1000 nm ($\epsilon \sim 100 \text{ L mol}^{-1} \text{ cm}^{-1}$) indicative for a Jahn-Teller distorted square pyramidal (or octahedral) structure (representative spectra and data are collected in the Supporting information) [30]. The energy of the ligand field absorptions for the Cu-OME containing compounds lie at somewhat lower energy (1097 nm/1033 nm) compared to the Cu-OH containing derivative (929 nm), reflecting a weaker ligand field imposed by the methoxy donor ligands compared to hydroxido. This points to ligand distortion around the copper ion, since weaker binding might be the result of a strained coordination geometry. The ligands exhibit strong bands in the UV range of the spectrum. The two bands discernible at around 270 and 310 nm are assigned to ligand-centred $\pi \rightarrow \pi^*$ transitions and do not shift markedly upon coordination (Table 6).

The first spectroelectrochemical experiments (using an optical transparent thin-layer electrode (OTTLE) cell) were devoted to demonstrate that the ligands tolerate the change in oxidation state of the copper atom from Cu^{II} to Cu^I. When reducing the parent complexes the blue colour of the ligand field transition vanishes, while the ligand-centred absorption bands decrease only slightly in intensity (5–30%) and the absorption maxima are virtually unchanged. Only the complex with the deprotonated ligand [(LOH)-CuCl(DMF)₂] exhibits a slight bathochromic shift (Table 6, for spectra see Supporting information). We thus conclude that coordination is retained upon reduction to Cu^I and the ligand easily follows the associated change of the coordination geometry. We assume that this can happen through the deformations (mainly rotation of the phenoxy substituent) discussed above.

The oxidation of the complexes occurs irreversibly as has been shown by cyclic voltammetry. Nevertheless, we studied the spectroscopic response upon oxidation. We found for all complexes

Table 5
Electrochemical data of free oxido-pincer ligands and their Cu^{II} and Ni^{II} complexes.^a

	E_{pa} ox/ligand	$E_{1/2}$ Cu ^I /Cu ^{II}	Solvent
<i>Ligands</i>			
LOH ₂	0.93		DMF
LOMe ₂	0.80		DMF
LOMe ₄	0.98		DMF
<i>Cu chlorido complexes</i>			
LOH ₂	1.01	-0.11	DMF
LOH ⁻	0.28	-0.03	DMF
LOMe ₂	0.90	-0.04	DMF
LOMe ₄	0.72	-0.01	DMF
<i>Cu(MeCN) complexes</i>			
LOMe ₄	1.54	0.21	MeCN
<i>Ni complexes^b</i>			
		E_{pa} Ni ^{II} /Ni ^{III}	
LOH ₂	0.82	0.41	THF
LOMe ₂	>1.04	0.56	THF
LOMe ₄	0.96	0.52	THF

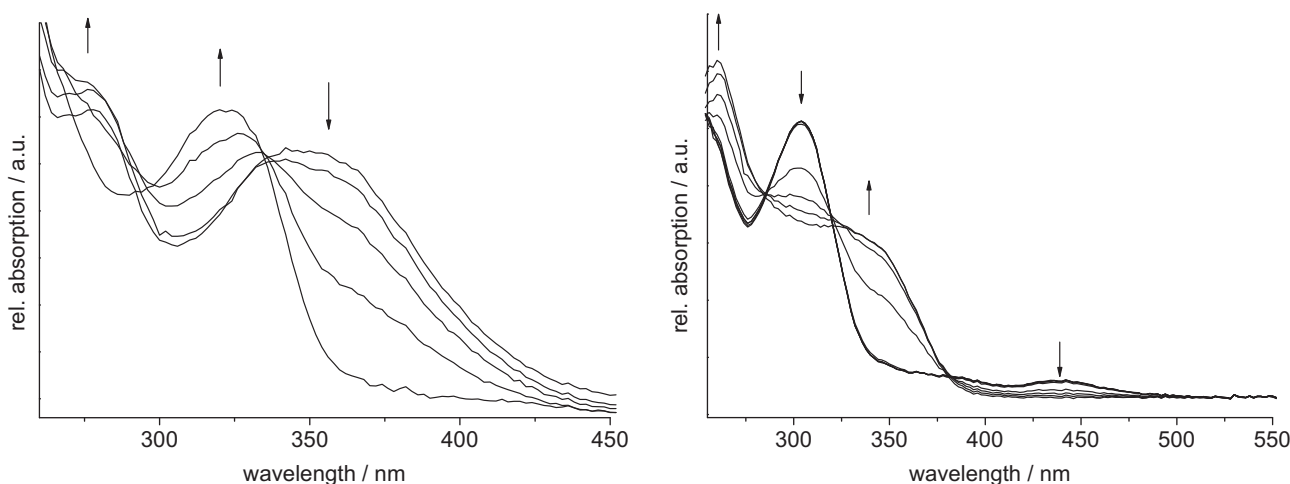
^a From cyclic voltammetry in *n*Bu₄NPF₆/solvent solutions; potentials in V vs. FeCp₂/FeCp₂⁺.

^b We assume that the nickel complexes are dimeric in THF solution.

Table 6

Data of absorption–titration experiments and spectroelectrochemical measurements in DMF, all bands in nm.

Titration	λ (nm)	Equivalents			
With CuCl ₂	278, 318, 436 ^a	0–5			
With CuCl ₂ (<i>n</i> Bu ₃ N as base)	278, 360	0–3			
Spectroelectrochemistry	Oxidation	Parent (Cu ^{II})	Cu ^{II} → Cu ^I	Reduction (I) ^b	Reduction (II) ^b
[(LOH)CuCl(DMF) ₂]	278, 322, 410sh	278, 343	277, 358		278, 351sh, 408
[(LOH ₂)CuCl ₂ (DMF)]	278, 316, 439	278, 316, 436 ^a	278, 318	278, 310, 425	278, 350sh, 408, 535
[(LOMe ₂)CuCl ₂ (DMF)]	258, 324, 342sh	258, 304	258, 306		
[(LOMe ₄)CuCl ₂ (DMF)]	264, 321, 371	264, 312	264, 314		

^a Assigned to [CuCl₄]²⁻.^b For experimental conditions see text.**Fig. 3.** Spectroelectrochemical measurement of oxidation processes at +1.0 V (vs. FeCp₂/FeCp₂⁺) in DMF/*n*Bu₄NPF₆ left: [(LOH)CuCl(DMF)₂]; right: [(LOMe₂)CuCl₂(DMF)]. Note, that the band at 436 nm, indicative for [CuCl₄]²⁻, also vanishes upon oxidation thus [CuCl₄]²⁻ is oxidised under these conditions.

quite similar spectra mainly characterised by a band at around 320 nm (for all complexes) and further long-wavelength bands varying from 340 to 440 nm, dependent on the ligand (Fig. 3). They can be assigned to the generation of phenoxy radical species [31], confirming our assignment of the waves around 1 V to ligand-based oxidations.

The LOH₂ ligand had been already analysed concerning its acid–base properties using absorption spectroscopy of the different (de)protonated species combined with calculations [13]. From this study we know that a band at 318 nm belongs to the protonated LOH₂ ligand (π – π^*). An absorption maximum of 349 nm indicates the singly deprotonated Ligand LOH⁻, while a band at 408 nm denotes the completely deprotonated LO²⁻ ligand. The absorption spectrum of the [(LOH₂)CuCl₂(DMF)] complex thus confirms that the ligand remains protonated upon coordination. However, it is reasonable to assume, that coordination of the LOH₂ ligand will strongly facilitate the deprotonation and we thus performed titration experiments (see Fig. 4, left) to investigate the pH-dependent behaviour of the metal complexes [32].

In a first experiment 0.3 mL *n*Bu₃N (1.3 mmol) were added to 3 mL of a solution of the LOH₂ ligand (0.6 mmol). Since no spectral changes were observed, we conclude that the free ligand is not deprotonated under these conditions. To this mixture small portions (10 μ L) of CuCl₂ in DMF were added. The corresponding absorption spectra showed a decreasing absorption at 318 nm (corresponding to the ligand LOH₂), while a new absorption band at 360 nm appeared (see Fig. 4, left). From the spectral fingerprint, we can assign the reaction to a deprotonation of the coordinated ligand (formation of LOH⁻). Further addition of base does not

change the spectrum, thus a fully deprotonated complex species, containing LO²⁻ is not accessible using *n*Bu₃N (pK_a = 10.9). Titration of the ligand LOH₂ under the same conditions without base leads to the formation of [(LOH₂)CuCl₂(DMF)], as indicated by an identical spectrum of the isolated complex (Table 6).

To establish if the complex [(LOH₂)CuCl₂(DMF)] is deprotonated upon reduction, as inferred from the CV experiments, we studied the complex by optical spectroelectrochemistry. Under reducing conditions (–2.7 V) the main absorption band of the complex [(LOH₂)CuCl₂(DMF)] at 318 nm vanishes while a new band appears at 425 nm (Fig. 4, right). Further reduction (–3.0 V) finally leads to a strong band at 408 nm. While the 408 nm band is unequivocally indicative for the doubly deprotonated ligand, the band at 425 nm is assigned to the species [(LOH)CuCl₂(DMF)]⁻. When studying the complex carrying the deprotonated ligand [(LOH)CuCl(DMF)₂] we observed the 408 nm band evolving immediately under reductive electrolysis. It is important to note, that reduction of [(LOH₂)CuCl₂(DMF)] and subsequent deprotonation in first instance leads to [(LOH)CuCl₂(DMF)]⁻ not to [(LOH)CuCl(DMF)₂], therefore the spectra are not identical (but very similar). Anyway our experiments give strong evidence, that the ligand-centred reduction processes of the complex [(LOH₂)CuCl₂(DMF)] are strongly coupled to deprotonation, which is unusual, as outlined in Section 2.6. This is further supported by the reductive spectroelectrochemistry of [(LOMe₂)CuCl₂(DMF)] and [(LOMe₄)CuCl₂(DMF)] where we did not observe any defined absorption bands upon reduction. A general overview of the titration experiments and spectroelectrochemical measurements is presented in Table 6, further representative figures are supplied in the Supporting information.

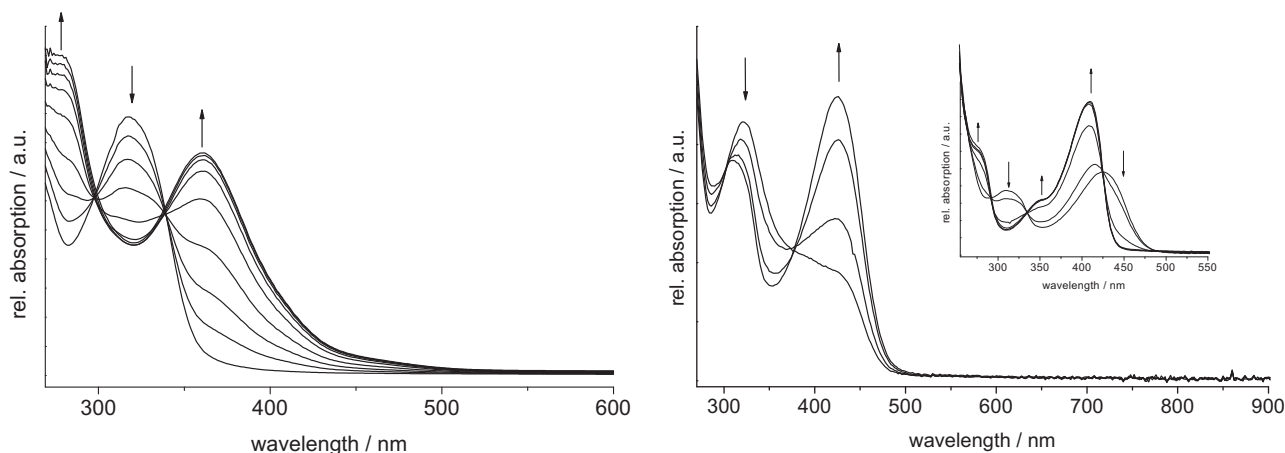


Fig. 4. Left: titration of a $\text{LOH}_2/n\text{Bu}_3$ solution with CuCl_2 in DMF; right: spectroelectrochemical reduction of $[(\text{LOH}_2)\text{CuCl}_2(\text{DMF})]$ in $\text{DMF}/n\text{Bu}_4\text{NPF}_6$ at -2.7 V (vs. $\text{FeCp}_2/\text{FeCp}_2^+$), the inset shows further reduction at -2.9 V presumably leading to $[(\text{LO})\text{CuCl}]^{2-}$.

3. Conclusions

A number of new binuclear Cu^{II} complexes containing bis-phenol-pyridine O,N,O-pincer ligands were synthesised, which can be reliably converted into mononuclear species $[(\text{O,N,O})\text{CuCl}_2(\text{DMF})]$ in DMF solution. These mononuclear compounds exhibit electrochemical behaviour comparable to natural oxidation catalysts as could be established from comparison with corresponding Ni^{II} complexes. The $\text{Cu}^{\text{II}}/\text{Cu}^{\text{I}}$ transformation occurs fully reversible at rather low potentials. Spectroelectrochemistry has allowed the *in situ* observation of the associated geometrical transformation of the coordination sphere around the copper ion. Furthermore, all three ligands form phenoxyl radicals. Unfortunately, these oxidations occur irreversibly at rather high potentials and were not comparable to natural co-factors in this respect. From our detailed titration experiments in combination with reductive spectroelectrochemistry we have strong evidence that the system $[(\text{LOH}_2)\text{CuCl}_2(\text{DMF})]$ exhibits a coupled reduction/deprotonation chemistry which would allow to generate deprotonated species electrochemically. The electrochemical and spectroscopic behaviour (absorption and emission) is fully in line with the assumption that the ligands offer a rather strained coordination geometry to the metal ions, comparable to those found in copper enzymes (entatic state).

4. Experimental

4.1. General

2,6-Dibromopyridine, 1,3-dimethoxybenzene, pyridinium hydrochloride and urea-hydrogen peroxide (UHP) were purchased from Aldrich. 2-Iodo-methoxybenzene was purchased from Alfa Aesar. $[\text{Ni}(\text{dppe})\text{Cl}_2]$ [33], $[\text{Ni}(\text{PPh}_3)\text{Br}_2]$ [34] were synthesised according to literature and 4-iodo-1,3-dimethoxybenzene in a modified synthesis [35]. The Grignard reactions and the Kumada-coupling reactions were carried out under inert gas conditions and performed by using Schlenk techniques. THF was dried using a MBRAUN MB SPS-800 solvent purification system.

4.2. Instrumentation

NMR spectra were recorded on a Bruker Avance II 300 MHz spectrometer, using a triple resonance ^1H , ^9BB inverse probe head. The unambiguous assignment of the ^1H and ^{13}C resonances was obtained from ^1H NOESY, ^1H COSY, gradient selected ^1H , ^{13}C HSQC

and HMBC experiments. All 2D NMR experiments were performed using standard pulse sequences from the Bruker pulse program library. Chemical shifts were relative to TMS. UV-Vis-NIR absorption spectra were measured on Varian Cary50 Scan or Shimadzu UV-3600 photo spectrometers. UV-Vis emission spectra were recorded with a Spex FluoroMax-3. Elemental analyses were carried out using a HEKAtech CHNS EuroEA 3000 Analyzer. EPR spectra were recorded in the X band on a Bruker System ELEXSYS 500E, with a Bruker Variable Temperature Unit ER 4131VT. *g* values were calibrated using a *dp*ph sample. Electrochemical experiments were carried out in 0.1 M $n\text{Bu}_4\text{NPF}_6$ solutions using a three-electrode configuration (glassy carbon electrode, Pt counter electrode, and Ag/AgCl reference) and an Autolab PGSTAT30 potentiostat and function generator. The ferrocene/ferrocenium couple ($\text{FeCp}_2/\text{FeCp}_2^+$) served as internal reference. UV-Vis spectroelectrochemical measurements were performed with an optical transparent thin-layer electrode (OTTLE) cell [36].

4.3. X-ray crystallographic studies

Crystal structure determinations were performed at 293(2) K using graphite-monochromatised Mo $K\alpha$ radiation ($\lambda = 0.71073\text{ \AA}$) on a IPDS II (STOE and Cie). The structures were solved by direct methods (SHELXS-97) [37] and refined by full-matrix least-squares techniques against F^2 (SHELXS-97) [38]. The numerical absorption corrections (X-RED V1.22; STOE and Cie, 2001) were performed after optimising the crystal shapes using X-SHAPE V1.06 (STOE and Cie, 1999) [39]. The non-hydrogen atoms were refined with anisotropic displacement parameters without any constraints. All H atoms of the free oxido-pincer ligands including the OH group were found during the refinement process.

4.4. Synthesis of the oxido-pincer ligands

4.4.1. 4-Iodo-1,3-dimethoxybenzene

1.38 g (10 mmol) 1,3-dimethoxybenzene were mixed with 1.27 g (5 mmol) I_2 (finely powdered) and 0.56 g (6 mmol) UHP (finely powdered). After exposing to ultrasound for 10 h, the mixture was extracted with 100 mL methyl *t*-butyl ether (MTBE). The organic phase was washed with an aqueous solution of Na_2SO_3 (10%) and then with water. After drying the MTBE-phase using MgSO_4 , the solvent was removed under reduced pressure to yield 2.62 g (99%) of a brown oil. ^1H NMR (300 MHz, CDCl_3): $\delta = 7.60$ (d, 1H, 5-Phen), 6.42 (d, 1H, 2-Phen), 6.31 (dd, 1H, 6-Phen), 3.84 (s, 3H, 3-OMe), 3.78 (s, 3H, 1-OMe) ppm. ^{13}C NMR (75 MHz, CDCl_3):

δ = 161 (1C, 1-Phen), 159 (1C, 3-Phen), 139 (1C, 5-Phen), 107 (1C, 6-Phen), 99 (1C, 2-Phen), 75 (1C, 4-Phen), 56 (1C, 3-OMe), 55 (1C, 1-OMe) ppm. $C_8H_9O_2I$ (264.06): *Anal. Calc.* C, 36.39; H, 3.44. Found: C, 36.30; H, 3.45%.

4.4.2. 2,6-Bis(2-methoxyphenyl)pyridine

11.7 g of 2-Iodo-methoxybenzene (50 mmol) were reacted with 1.8 g (75 mmol) magnesium in THF to give the Grignard component. The resulting solution was added dropwise to a stirred solution of 2,6-dibromopyridine and [(dppe)NiCl₂] (10 mol%) the reaction mixture was stirred for 12 h and the brown solution was quenched with 150 mL half concentrated HCl. After phase separation, the aqueous phase was extracted with CH₂Cl₂. The volume of the combined organic solutions was reduced and the product was precipitated by adding saturated ammonium chloride solution. The obtained solid was pale yellow. Yield 5.47 g (78%). Mp = 130 °C. ¹H NMR (300 MHz, CDCl₃): δ = 7.93 (dd, 2H, 6-Phen), 7.76 (m, 3H, 3,4,5-Py), 7.36 (t, 2H, 4-Phen), 7.14 (d, 2H, 3-Phen), 7.07 (t, 2H, 5-Phen), 3.88 (s, 6H, OMe) ppm. ¹³C NMR (75 MHz, CDCl₃): δ = 158 (2C, 2-Phen), 155 (2C, 2,6-Py), 135 (1C, 4-Py), 132 (2C, 6-Phen), 130 (2C, 4-Phen), 123 (2C, 3,5-Py), 121 (4C, 1,5-Phen.), 112 (2C, 3-Phen), 55 (2C, 2-OMe) ppm. $C_{19}H_{17}NO_2$ (291.34): *Anal. Calc.* C, 78.33; H, 5.88; N, 4.81. Found: C, 78.33; H, 5.85; N, 4.82%.

4.4.3. 2,6-Bis(2-hydroxyphenyl)pyridine

A mixture of 0.50 g (1.7 mmol) 2,6-bis(2-methoxyphenyl)pyridine and 5.18 g (44 mmol) pyridinium hydrochloride was heated up to 190 °C and was stirred for 1 h. The resulting yellow-green solution was cooled down to room temperature, where the liquid solidified. The solid was suspended in water using an ultrasonic bath. The suspension was extracted several times using a total of 400 mL CH₂Cl₂. The combined organic phases were washed with a saturated sodium carbonate solution and dried over anhydrous Na₂SO₄. After filtration the solvent was removed under vacuum to leave a beige solid. Yield 344 mg (76%). Mp = 139 °C. ¹H NMR (300 MHz, CDCl₃): δ = 9.88 (s (br), 2H, OH), 8.00 (t, 1H, 4-Py), 7.72 (d, 2H, 3,5-Py), 7.69 (d, 2H, 6-Phen), 7.35 (t, 2H, 4-Phen), 7.05 (d, 2H, 3-Phen), 7.00 (t, 2H, 5-Phen) ppm. ¹³C NMR (75 MHz, CDCl₃): δ = 156 (2C, 2-Phen), 151 (2C, 2,6-Py), 140 (1C, 4-Py), 132 (2C, 4-Phen), 128 (2C, 6-Phen), 121 (2C, 1-Phen), 120 (4C, 3,5Py,5-Phen), 118 (2C, 3-Phen) ppm. $C_{17}H_{13}NO_2$ (263.30): *Anal. Calc.* C, 77.55; H, 4.98; N, 5.32. Found: C, 77.54; H, 4.99; N, 5.31%.

4.4.4. 2,6-Bis-(2,4-dimethoxyphenyl)pyridine magnesium bromide [(LOMe₄)MgBr₂]

A Grignard reagent was prepared from 12.5 g (47 mmol) 4-iodo-1,3-dimethoxybenzene and 2.0 g (excess) magnesium in THF. The Grignard-solution was added slowly to a solution of 5.57 g (23.5 mmol) 2,6-dibromo-pyridine and 0.97 g (8 mol%) [(dppe)NiCl₂] in dry THF at 0 °C. The reaction mixture was stirred at 0 °C overnight. After 12 h the reaction was stopped by adding 150 mL of HCl/water (1:1) and the reaction product was precipitated by adding 400 mL of CH₂Cl₂. The bright yellow solid was filtered off and washed with a small portion of cold acetone. The product was dried at 60 °C and then stored in a brown glass vessel to prevent the yellow solid from turning dark orange. Yield: 8.03 g (98%). ¹H NMR (300 MHz, [D₆]-acetone): δ = 8.63 (t, 1H, 4-Py), 8.29 (d, 2H, 3,5-Py), 8.01 (d, 2H, 6-Phen), 6.93 (d, 2H, 5-Phen), 6.87 (dd, 2H, 3-Phen), 4.19 (s, 6H, 2-OMe), 3.88 (s, 6H, 4-OMe) ppm. ¹³C NMR (75 MHz, [D₆]-acetone): δ = 167 (2C, 4-Phen), 161 (2C, 2-Phen), 151 (2C, 2,6-Py), 146 (1C, 4-Py), 133 (2C, 3-Phen), 123 (2C, 3,5-Py), 108 (2C, 6-Phen), 101 (2C, 1-Phen), 100 (2C, 5-Phen), 57 (4C, 2,4-OMe) ppm. $C_{21}H_{21}NO_4MgBr_2$ (535.52): *Anal. Calc.* C, 47.10; H, 3.95; N, 2.62%. Found: C, 47.13; H, 4.02; N, 2.61%.

4.4.5. 2,6-Bis-(2,4-dimethoxyphenyl)pyridine

3.0 g (5.2 mmol, 1 eq) of [(LOMe₄)MgBr₂] were suspended in ethyl acetate and an aqueous solution of 1.0 g Kryptofix-® (2.2.2) was added until all starting material has dissolved. Then the phases were separated and the organic phase was subsequently washed with two small portions of Kryptofix solution. After final phase separation the organic phase was dried over anhydrous Na₂SO₄. After filtration the solvent was removed under vacuum leaving a yellow-orange solid. Yield 1.57 g (87%). ¹H NMR (300 MHz, [D₆]-acetone): δ = 8.01 (d, 2H, 6-Phen), 7.79 (d, 2H, 3,5-Py), 7.69 (t, 1H, 4-Py), 6.68 (m, 4H, 5,6-Phen), 3.91 (s, 6H, 2-OMe), 3.87 (s, 6H, 4-OMe) ppm. ¹³C NMR (75 MHz, [D₆]-acetone): δ = 163 (2C, 4-Phen), 160 (2C, 2-Phen), 156 (2C, 2,6-Py), 135 (1C, 4-Py), 132 (2C, 6-Phen), 135 (2C, 3,5-Py), 105 (2C, 5-Phen), 10 (2C, 1-Phen), 98 (2C, 3-Phen), 55 (4C, 2,4-OMe) ppm. $C_{21}H_{21}NO_4$ (351.41): *Anal. Calc.* C, 71.78; H, 6.02; N, 3.99. Found: C, 71.63; H, 6.05; N, 4.00%.

4.5. Synthesis of the oxido-pincer complexes

4.5.1. Tetrakis(acetonitrile)copper(II) bis(trifluoroacetate)

[Cu(MeCN)₄(TFA)₂]

2.0 g (15 mmol) anhydrous CuCl₂ was dissolved in 100 mL acetonitrile and 20 mL trifluoroacetic acid and refluxed over night. The remaining solution was evaporated to 50 mL and the product was precipitated at -25 °C as a blue fine-crystalline solid. Yield 4.30 g (63%). $C_{12}H_{12}F_6N_4O_4Cu$ (453.81): *Anal. Calc.* C, 31.76; H, 2.67; N, 12.35. Found: C, 31.74; H, 2.66; N, 12.33%.

4.5.2. Dichlorido(2,6-bis(2-methoxyphenyl)pyridine)copper(II)

[(LOMe₂)CuCl₂]₂

200 mg LOMe₂ (0.69 mmol) and 92 mg (0.69 mmol) anhydrous CuCl₂ were separately dissolved in 5 mL methanol and the copper solution was added slowly to the ligand solution. The reaction mixture was stirred at room temperature over night. The solvent was removed under vacuum and the remaining orange-brown solid was washed with a small portion cold acetone and dried. Yield 210 mg (71%). $C_{19}H_{17}NO_2CuCl_2$ (425.80): *Anal. Calc.* C, 53.60; H, 4.02; N, 3.29. Found: C, 53.57; H, 4.00; N, 3.30%.

4.5.3. Dichlorido(2,6-bis(2-hydroxyphenyl)pyridine)copper(II)

[(LOH₂)CuCl₂]₂

0.20 g (0.76 mmol) LOH₂ and 0.10 g anhydrous CuCl₂ were dissolved separately in 5 mL methanol. Both solutions were combined and stirred at room temperature for 12 h. After removing the solvent under vacuum a black solid was obtained. Yield: 211 mg (72%). $C_{17}H_{13}NO_2CuCl_2$ (397.75): *Anal. Calc.* C, 51.34; H, 3.29; N, 3.52. Found: C, 51.28; H, 3.29; N, 3.51%.

4.5.4. Chlorido(2-(2-hydroxyphenyl)-6-(hydroxyphenyl)pyridine)

copper(II) [(LOH)CuCl]₂

50 mg (0.13 mmol) of [(LOH₂)CuCl₂] were dissolved in 7 mL methanol and 0.5 mL NEt₃ were added. A green-brown solid precipitated immediately and was filtered off. Yield 35 mg (77%). $C_{17}H_{12}NO_2CuCl$ (361.29): *Anal. Calc.* C, 56.52; H, 3.35; N, 3.88. Found: C, 56.52; H, 3.38; N, 3.89%.

4.5.5. Dichlorido(2,6-bis-(2,4-dimethoxyphenyl)pyridine)copper(II)

[(LOMe₄)CuCl₂]₂

0.20 g (0.58 mmol) LOMe₄ and 78 mg (0.58 mmol, 1 eq) anhydrous CuCl₂ were dissolved separately in 5 mL methanol. Both solutions were combined and stirred at room temperature for 2 days. Removing the solvent from the mixture yielded a brown solid, which was washed with a small amount of cold acetone and dried on air. Yield (190 mg, 60%). $C_{42}H_{42}N_2O_8Cu_2Cl_4$ (971.71): *Anal. Calc.* C, 51.91; H, 4.36; N, 2.88. Found: C, 51.89; H, 4.33; N, 2.88%.

4.5.6. Bis(trifluoroacetato)(2,6-bis-(2,4-dimethoxyphenyl)pyridine)copper(II) [(LOMe₄)Cu(TFA)₂]

179 mg (0.29 mmol, 1.5 eq) [Cu(MeCN)₄](TFA)₂ and 100 mg (0.19 mmol, 1 eq) [(LOMe₄)MgBr₂] were mixed as solids and dissolved in 15 mL acetonitrile. The green solution was stirred for 6 h at room temperature then the acetonitrile was removed under vacuum leaving a dark green solid. Yield 103 mg (84%). C₂₅H₂₁NO₈·CuF₆ (641.00): *Anal. Calc.* C, 46.84; H, 3.30; N, 2.19. Found: C, 46.82; H, 3.33; N, 2.20%.

4.5.7. Dibromido(2,6-bis(2-methoxyphenyl)pyridine)nickel(II) [(LOMe₂)NiBr₂]₂

85 mg (0.29 mmol, 1 eq) of LOMe₂ were dissolved in 7 mL methanol. A methanolic solution of 215 mg (0.29 mmol, 1 eq) [(PPh₃)₂NiBr₂] (7 mL) was added in one portion and the resulting mixture was stirred for 6 h. The solvent was removed under vacuum and the remaining turquoise solid was washed with small portions of cold acetone and dried, Yield 98 mg (45%). ¹H NMR (300 MHz, [D₆]-acetone): δ = 8.52 (t, 1H, 4-Py), 8.30 (d, 2H, 3,5-Py), 8.04 (d, 2H, 6-Phen), 7.59 (t, 2H, 4-Phen), 7.35 (t, 2H, 5-Phen), 7.22 (d, 2H, 3-Phen), 4.10 (s (br), 6H, OMe) ppm. C₁₉H₁₇NO₂NiBr₂ (509.86): *calcd.* C 44.76, H 3.36, N 2.75; *found:* C 44.75, H 3.35, N 2.74.

4.5.8. Dibromido(2,6-bis(2-hydroxyphenyl)pyridine)nickel(II) [(LOH₂)NiBr₂]₂

75 mg (0.30 mmol, 1 eq) of LOH₂ were dissolved in 7 mL methanol. A methanolic solution of 223 mg (0.30 mmol, 1 eq) [(PPh₃)₂NiBr₂] (7 mL) was added in one portion and the resulting mixture was stirred for 6 h. The solvent was removed under vacuum and the remaining green solid was washed with small portions of cold acetone and then dried. Yield 106 mg (47%). ¹H NMR (300 MHz, [D₆]-acetone): δ = 11.67 (s (br), 2H, OH), 8.00 (m, 3H, 3,4,5-Py), 7.86 (dd, 2H, 6-Phen), 7.32 (t, 2H, 4-Phen), 7.00 (m, 2H, 3,5-Phen) ppm. C₁₇H₁₃NO₂NiBr₂ (481.81): *Anal. Calc.* C, 42.38; H, 2.72; N, 2.91. Found: C, 42.36; H, 2.75; N, 2.88%.

4.5.9. Dibromido(2,6-bis-(2,4-dimethoxyphenyl)pyridine)nickel(II) [(LOMe₄)NiBr₂]₂

100 mg (0.19 mmol, 1 eq) of [(LOMe₄)MgBr₂] were dissolved in 7 mL methanol. A methanolic solution of 215 mg (0.29 mmol, 1.5 eq) [(PPh₃)₂NiBr₂] (7 mL) was added in one portion and the resulting mixture was stirred for 6 h. The solvent was removed under vacuum and the remaining yellow-green solid was washed with small portions of cold acetone and subsequently dried. Yield 83 mg (79%). ¹H NMR (300 MHz, [D₆]-acetone): δ = 8.94 (t, 1H, 4-Py), 8.55 (d, 2H, 3,5-Py), 8.18 (d, 2H, 6-Phen), 7.04 (d, 2H, 5-Phen), 7.00 (d, 2H, 6-Phen), 4.40 (s, 6H, 2-OMe), 4.05 (s, 6H, 4-OMe) ppm. C₂₁H₂₁NO₄NiBr₂ (569.92): *Anal. Calc.* C, 44.26; H, 3.71; N, 2.46. Found: C, 44.26; H, 3.70; N, 2.48%.

Acknowledgments

Dr. I. Pantenburg and I. Müller from the University of Cologne are thanked for the X-ray measurements. A. Kaiser is acknowledged for the synthesis of the nickel catalyst for the C–C-coupling. We also would like to thank the “Studienstiftung des Deutschen Volkes” for financial support.

Appendix A. Supplementary material

CCDC 751119 and 751120 contain the supplementary crystallographic data for this paper. These data can be obtained free of charge from The Cambridge Crystallographic Data Centre via www.ccdc.cam.ac.uk/data_request/cif. Supplementary data (crystal data on LOMe₂ and LOMe₄ and a table on absorption measure-

ments. Additional figures show the π-stacking in the crystal structure of LOMe₄, representative cyclic voltammograms, emission spectra and UV–Vis-spectroelectrochemical experiments) associated with this article can be found, in the online version, at [doi:10.1016/j.ica.2010.06.011](https://doi.org/10.1016/j.ica.2010.06.011).

References

- (a) M.R. Redinbo, D. Cascio, M.K. Choukair, D. Rice, S. Merchant, T.O. Yeates, *Biochemistry* 32 (1993) 10560; (b) R. Huber, *Angew. Chem.* 101 (1989) 849; *Angew. Chem., Int. Ed.* 28 (1989) 848.
- N. Ito, S.E.V. Phillips, C. Stevens, Z.B. Ogel, M.J. McPherson, J.N. Keen, K.D.S. Yadav, P.F. Knowles, *Nature* 350 (1991) 87.
- E.I. Solomon, U.M. Sundaram, T.E. Machonkin, *Chem. Rev.* 94 (1994) 737.
- (a) G.C.M. Steffens, R. Bielwald, G. Buse, *Eur. J. Biochem.* 164 (1987) 295; (b) G.C.M. Steffens, T. Soulimane, G. Wolff, G. Buse, *Eur. J. Biochem.* 213 (1993) 1149.
- (a) F. Himo, L.A. Eriksson, F. Maseras, P.E.M. Siegbahn, *J. Am. Chem. Soc.* 122 (2000) 8031; (b) J.W. Whittaker, *Chem. Rev.* 103 (2003) 2347.
- (a) A.G. Sykes, *Adv. Inorg. Chem.* 36 (1991) 377; (b) H.E.M. Christensen, L.S. Conrad, K.V. Mikkelsen, M.K. Nielsen, *J. Ulstrup, Inorg. Chem.* 29 (1990) 2808.
- W. Kaim, *Dalton Trans.* (2003) 761.
- N.G. Connelly, W.E. Geiger, *Chem. Rev.* 96 (1996) 877.
- (a) B.L. Vallee, R.J.P. Williams, *Proc. Natl. Acad. Sci. USA* 59 (1968) 498; R.J.P. Williams, *J. Mol. Catal. (Review issue)* (1986) 1.
- (a) K.M. Merz, R. Hoffmann, *Inorg. Chem.* 27 (1988) 2120; (b) M. Hakansson, S. Jagner, E. Clot, O. Eisenstein, *Inorg. Chem.* 31 (1992) 5389.
- K.D. Karlin, Y. Gultneh, *Prog. Inorg. Chem.* 35 (1987) 219.
- A. Klein, S. Elmas, K. Butsch, *Eur. J. Inorg. Chem.* (2009) 2271.
- S. Steinhäuser, U. Heinz, J. Sander, K. Hegetschweiler, *Z. Anorg. Allg. Chem.* 630 (2004) 1829.
- W. Kaim, A. Klein, *Spectroelectrochemistry*, RCS Publishing, Cambridge, UK, 2008.
- H.-Y. Zhang, K.-Q. Ye, J.-Y. Zhang, Y. Liu, Y. Wang, *Inorg. Chem.* 45 (2006) 1745.
- A.M.S. Silva, L.M.P.M. Almeida, J.A.S. Cavaleiro, C. Foces-Foces, A.L. Llamas-Saiz, C. Fontenas, N. Jagerovic, J. Elguero, *Tetrahedron* 53 (1997) 11645.
- Although the goodness of fit is not very good there is no doubt on the applied space group P2₁2₁2₁ (concluded from its typical extinctions). The Flack parameter is not relevant in our case; compare also H.D. Flack, G. Bernadinelli, *J. Appl. Cryst.* 33 (2000) 1143.
- E. Ludwig, U. Schilde, E. Uhlemann, H. Hartl, I. Briidgam, *Z. Anorg. Allg. Chem.* 622 (1996) 701.
- I.A. Koval, M. Sgobba, M. Huisman, M. Lünen, E. Saint-Aman, P. Gamez, B. Krebs, J. Reedijk, *Inorg. Chim. Acta* 359 (2006) 4071.
- B.J. Hathaway, D.E. Billing, *Coord. Chem. Rev.* 5 (1970) 143.
- P. Kapoor, A. Pathak, R. Kapoor, P. Venugopalan, M. Corbella, M. Rodríguez, J. Robles, A. Lobet, *Inorg. Chem.* 41 (2002) 6153.
- S. Thakurta, P. Roy, G. Rosair, C.J. Gómez-García, E. Garribba, S. Mitra, *Polyhedron* 28 (2009) 695.
- F. Yraola, F. Albericio, M. Corbella, M. Royo, *Inorg. Chim. Acta* 361 (2008) 2455.
- A. Bencini, D. Gatteschi, *Inorg. Chim. Acta* 31 (1978) 11.
- D. Reinen, C. Friebel, *Inorg. Chem.* 23 (1984) 791.
- (a) N. Wei, N.N. Murthy, K.D. Karlin, *Inorg. Chem.* 33 (1994) 6093; G. Kokoszka, K.D. Karlin, F. Padula, J. Baranowski, C. Goldstein, *Inorg. Chem.* (1984) 4378.
- A.W. Addison, H.M.J. Hendriksen, J. Reedijk, L.K. Thompson, *Inorg. Chem.* 20 (1981) 103.
- T. Glowiak, I. Podgorska, *Inorg. Chim. Acta* 125 (1986) 83.
- Y. Wang, T.D.P. Stack, *J. Am. Chem. Soc.* 118 (1996) 13097.
- C. Furlani, *Coord. Chem. Rev.* 3 (1968) 141.
- M.R. Ganapathi, R. Hermann, S. Naumov, Ortwin Brede, *Phys. Chem. Chem. Phys.* 2 (2000) 4947.
- (a) A. Jansc, Z. Paks, N. Jakab, B. Gyurcsik, A. Rockenbauer, T. Gajda, *Dalton Trans.* (2005) 3187; (b) Z. Paks, A. Jansc, F. Pacello, N. Nagy, A. Battistone, T. Gajda, *J. Inorg. Biochem.* 102 (2008) 1700; (c) A. Pérez-Cadenas, L. Godino-Salido, R. López-Garzón, P. Arranz-Mascarós, D. Gutiérrez-Valero, R. Cuesta-Martos, *Transition Met. Chem.* 26 (2001) 581.
- K. Matsumoto, N. Kotoku, T. Shizuka, R. Tanaka, S. Okeya, *Inorg. Chim. Acta* 321 (2001) 167.
- J. Chatt, B.L. Shaw, *J. Chem. Soc.* (1960) 1718.
- J. Pavlinac, M. Zupan, S. Stavber, *Org. Biomol. Chem.* 5 (2007) 699.
- M. Krejčík, M. Daňek, F. Hartl, *J. Electroanal. Chem.* 317 (1991) 179.
- G.M. Sheldrick, SHELXS-97: A Program for Crystal Structure Solving, University of Göttingen, 1997.
- G.M. Sheldrick, SHELXL-97: A Program for the Refinement of Crystal Structures, University of Göttingen, 1997.
- (a) STOE X-RED, Data Reduction Program, Version 1.22/Windows, STOE and Cie, Darmstadt, 2001.; (b) STOE X-SHAPE, Crystal Optimisation for Numerical Absorption Correction, Version 1.06/Windows, STOE and Cie, Darmstadt, 1999.